ACS central science

Research Article

http://pubs.acs.org/journal/acscii

Synthesis, Properties, and Design Principles of Donor−Acceptor Nanohoops

Evan R. Darzi, Elizabeth S. Hirst, Christopher D. Weber, Lev N. Zakharov, Mark C. Lonergan, and Ramesh Jasti*

Department of Chemistry and Biochemistry, University of Oregon, Eugene, Oregon 97403, United States

Supporting Information

ABSTRACT: We have synthesized a series of aza[8]cycloparaphenylenes containing one, two, and three nitrogens to probe the impact of nitrogen doping on optoelectronic properties and solid state packing. Alkylation of these azananohoops afforded the first donor−acceptor nanohoops where the phenylene backbone acts as the donor and the pyridinium units act as the acceptor. The impact on the optoelectronic properties was then studied experimentally and computationally to provide new insight into the effect of functionalization on nanohoops properties.

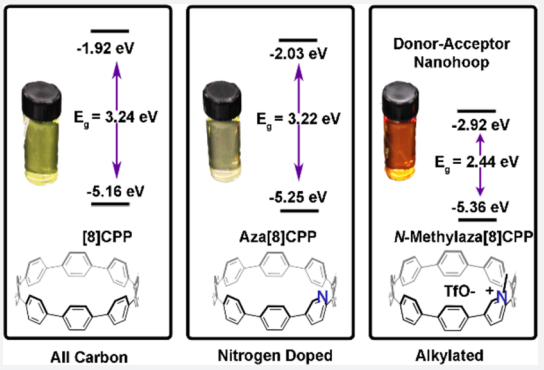

INTRODUCTION

Alternative energy technologies are needed to address increasing worldwide energy demands.[1] Organic materials are poised to play a significant role in these technologies with research focusing on their ability to harvest (organic photovoltaics, OPVs), transport (organic field-effect transistors, OFETs, and molecular wires), and store energy (batteries and capacitors).[2] Research in polymeric and small molecule based organic electronics has received a dramatic upsurge in recent years for their potential use as lightweight and flexible electronic materials.[3] Organic small molecules are relatively cheap, structurally defined, and can be functionalized to systematically study structure−property relationships. Although many strides have been made in the small molecules used to this end, the scaffold diversity is still low with the majority of research focusing on fullerene, oligothiophene, or acene-like motifs. With an understanding of the fundamental phenomena governing charge transport emerging, a more diverse toolbox of organic scaffolds is needed to guide future materials research.[4]

[*n*]Cycloparaphenylenes ([*n*]CPPs) possess a unique architecture of fully conjugated bent benzenes linked in the para position to form a nanohoop.[5] This nanohoop architecture imparts several advantageous properties in relation to their linear counterparts. First, they have a narrowing highest occupied molecular orbital (HOMO)−lowest unoccupied molecular orbital (LUMO) energy gap as the number of benzene units is decreased. This trend is in stark contrast to linear conjugated materials, including poly(*para*-phenylenes) (PPPs), which have a narrowing HOMO−LUMO energy as the molecule becomes larger.[6] Figure 1 illustrates this dramatic effect where the HOMO−LUMO energy gap for PPPs are comparable to [18]CPP but over an electronvolt (eV) larger than that of [5]CPP.[7] The calculated energy level deviation can be explained by a strain-induced minimization of the biaryl dihedral angles as the nanohoops become smaller,[8] which effectively increases conjugation around the hoop. In addition, the smaller nanohoops have increased quinoidal character,[9] which is also advantageous for charge transport in conjugated systems. Another advantage is the unique solid-state architecture of these compounds which pack into long-range channels with multiple close $\pi-\pi$ contacts. The curved nature of these nanohoops also affords a significant increase in solubility without the need for additional solubilizing chains.[10] Finally, the cyclic "infinite" conjugation afforded by the nanohoops framework renders them electronic hybrids between polymers and small molecules.

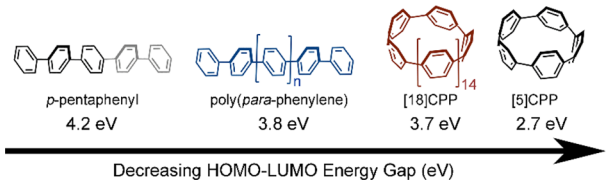

Figure 1. Wrapping a linear polymer into a cyclic isomer leads to dramatic modulation of the electronic structure. Calculated HOMO−LUMO energy gaps are taken from ref 7.

Significant effort has been devoted to altering the electronic properties of carbon materials, better tailoring them to specific applications. Doping of materials with a noncarbon element such as nitrogen, boron, phosphorus, or silicon has been one

Received: July 28, 2015
Published: September 3, 2015

DOI: 10.1021/acscentsci.5b00269
ACS Cent. Sci. 2015, 1, 335−342

approach to modify properties.[11] Nitrogen doping in particular has been shown to not only enable tuning of electronics but also introduce novel reactivity into these materials. The top-down synthesis of nitrogen-doped carbon nanotubes (CNTs) has led to significant modulation of various properties. Top-down nitrogen doping techniques, however, lead to a number of possible structures as illustrated in Figure 2a making direct

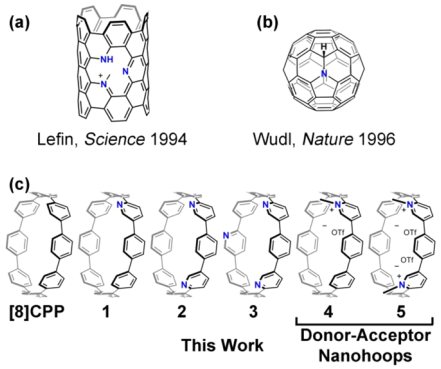

Figure 2. (a) Nitrogen doped CNT. (b) Azafullerene. (c) Targeted compounds **1** aza[8]CPP, **2** 1,15-diaza[8]CPP, **3** 1,15,31-triaza[8]-CPP, **4** *N*-methylaza[8]CPP triflate, and **5** *N*,*N*-dimethyl-1,15-diaza[8]CPP ditriflate.

structure–property relationships difficult to study. Bottom-up organic chemistry approaches, on the other hand, such as those used to access azafullerene (Figure 2b), have allowed in-depth studies of these "doped" systems and have facilitated the design of new materials.[12] Although heteroatom incorporation in carbon nanohoops has previously been achieved,[13] donor–acceptor systems have not been investigated.[14] Herein, we report the bottom-up synthesis of a family of aza[8]CPPs and their donor–acceptor alkylated counterparts—structures in which the pyridinium unit serves as an electron-poor acceptor, and the bent phenylene unit is the electron-rich donor (Figure 2c). The effects of structural modifications on optical and electronic properties are presented in the context of experimental and computational studies. In addition, we provide a platform for the design of future donor–acceptor nanohoops with tailored electronic and optical properties.

RESULTS AND DISCUSSION

Synthesis of Aza- and Donor–Acceptor Nanohoops. Synthesis of nitrogen-doped CPPs was achieved by a scalable and modular route that leverages the inherent orthogonal reactivity of aryl chlorides and bromides to lithium halogen exchange. The synthesis relies on the construction of a dihalo or diboronate macrocyclic precursors containing oxidatively dearomatized cyclohexadiene moieties as masked arenes.[17] Macrocylization is then achieved by Suzuki-Miyaura cross-coupling reactions followed by a reductive aromatization step to achieve the final nitrogen doped nanohoop structures. The synthesis of key three-ring intermediates **8a–e** is summarized in Scheme 1 and began with the addition of either 4-chlorophenyllithium, 4-bromophenyllithium, 6-chloro-3-pyridinyllithium, or 6-bromo-3-pyridinyllithium to benzoquinone monoketal followed by acid-catalyzed ketal deprotection to give aryl quinols **7a–d** in moderate to excellent yields. Quinols **7a–d** were then deprotonated with sodium hydride and subjected to nucleophilic addition by the appropriate lithio haloarene to give the *syn* three-ring fragments **8a–e** after *in situ* alkylation with methyl iodide. Note that regioselective lithiation of 2,5-dibromopyridine was selectively achieved in the 5-position under kinetic control in coordinating solvents such as THF as detailed by Wang et al.[18] X-ray crystallographic analysis of **8e** confirmed the position of the nitrogen atoms and the *syn* configuration of the arenes (Supplementary Figure 1). Compounds **8a** and **8c** were then treated with *n*-butyllithium and quenched with quinone monoketal followed by acid catalyzed ketal deprotection to give four-ring quinols **9a** and **9b**

Scheme 1. Synthesis of [8]CPP and Targets aza[8]CPPs 1–3 and Donor–Acceptor aza[8]CPPs 4 and 5

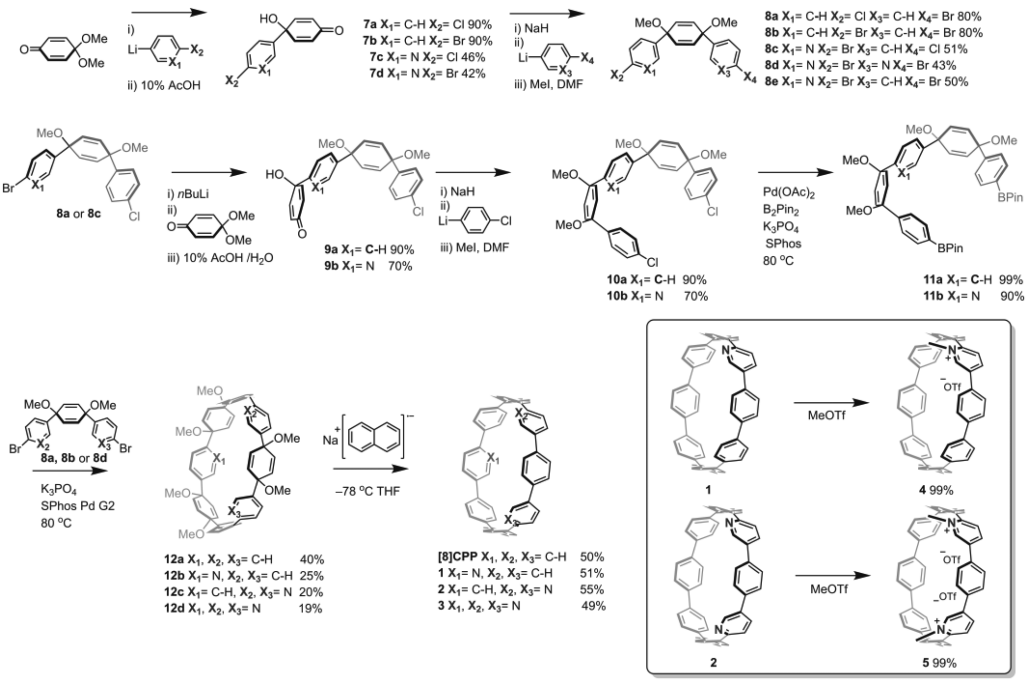

DOI: 10.1021/acscentsci.5b00269
ACS Cent. Sci. 2015, 1, 335–342

respectively. Quinols **9a** and **9b** were then treated with sodium hydride and subjected to nucleophilic addition of 4-bromophenyllithium followed by alkylation with methyl iodide to afford five-ring dichlorides **10a** and **10b**. Five-ring dichlorides **10a** and **10b** were then transformed to the corresponding bisboronates **11a** and **11b** through a Miyaura borylation with $Pd(OAc)_2$, SPhos, and B_2Pin_2. The iterative construction of the macrocyclic precursors allows for the possibility of the introduction of a wide variety of heteroaromatics at varying positions.

Suzuki-Miyaura cross-coupling of five-ring bisboronates (**11a** or **11b**) and three-ring dibromides (**8a**, **8b**, or **8d**) was achieved using Buchwald's second generation SPhos precatalyst to give macrocycles **12a–d** in moderate yield (Scheme 1). These macrocycles were then subjected to sodium napthalenide at −78 °C to give [8]CPP, aza[8]CPP (**1**), 1,15-diaza[8]CPP (**2**), and 1,15,31triaza[8]CPP (**3**). Aza-CPPs **1** and **2** were then treated with methyl triflate in dry dichloromethane to afford the donor–acceptor monoalkylated *N*-methylaza[8]CPP triflate **4** and *N*,*N*-dimethyle-1,15-diaza[8]CPP ditriflate **5** quantitatively. Peralkylation of triaza[8]CPP **3** did not cleanly afford *N*,*N*,*N*-trimethyl-1,15,31-triaza[8]CPP tritriflate, but rather a complex mixture of inseparable and unidentifiable compounds. Compounds **1–5** were thoroughly characterized using ^1H and ^{13}C NMR spectroscopy and mass spectrometry (see Supporting Information).

Solid-State Packing Morphology of Aza- and Donor–Acceptor Nanohoops. Single-crystal X-ray structure determination was performed on compounds **1** and **5**. Figure 3 shows the ORTEP, packing structure, and unique interactions for each compound. Packing motifs of organic materials are critical for understanding intermolecular charge transport.[4] We were curious to how nitrogen incorporation would affect the nanohoop solid-state packing that is typically observed. The nitrogen in **1** is found to be disordered over all 32 possible locations in the solid state. The impact of simple nitrogen incorporation into the [8]CPP backbone is menial and results in a nearly identical herringbone crystal packing observed for [8]CPP in previous reports (Supplementary Figure 4).[17b] Attempts were made to order the nitrogen distribution in the solid state using cocrystallants; however these efforts resulted in similar disorder. In contrast, compound **5** had a dramatically different packing structure compared to **1–3** and any previously reported [*n*]CPP. Donor–acceptor nanohoop **5** was found to be ordered adopting a *trans* relationship for the *N*-methylpyridinium triflate rings. Each nanohoop in the crystal structure has one face centered donor–acceptor interaction between its own pyridinium ring and a neighbor's electron-rich phenylene ring. The shortest contacts between these neighboring subunits is 3.35 Å and is highlighted in Figure 3c. This head to tail packing results in a 2D plane as shown in Figure 3b. The layers that make up the third dimension of the crystal structure form tubular channels similar to those seen in the solid state packing of [6]CPP.[19] Although the charge transport in nanohoops has not been explored yet, access to multiple packing motifs will help guide future design. The dipole moments of these alkylated nanohoops (SI Computational Coordinates) far exceed any previously reported nanohoops and serve as a new supramolecular design motif for their solid-state structures.

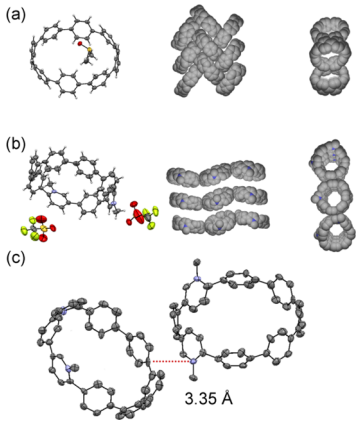

Figure 3. ORTEP, side-on packing, and top down packing of (a) **1** and (b) **5**. (c) Head to tail interaction between one pyridinium acceptor and a neighboring electron-rich phenylene donor in compound **5**.

Electrochemical Properties of Aza- and Donor–Acceptor Nanohoops. A primary goal of this study was to effectively lower the LUMO energy to levels more appropriate for functional electronic materials such as the n-type semiconductor C_{60}. Cyclic voltammetry (CV) was used to probe the reduction properties of [8]CPP and compounds **1–5**. Oxidations fell outside of the solvent window and thus were not reported. The cathodic peak potentials for the reduction of [8]CPP and **1–3** were recorded as −2.44 V, −2.39 V, −2.32 V, and −2.39 V respectively versus the ferrocene/ferrocenium couple. Compound **4** has a cathodic peak potential at −1.49 V, while **5** had two reduction events with peak potentials recorded at −1.36 V and −1.49 V versus the ferrocene/ferrocenium couple. The voltammograms for these compounds are illustrated in Figure 4.

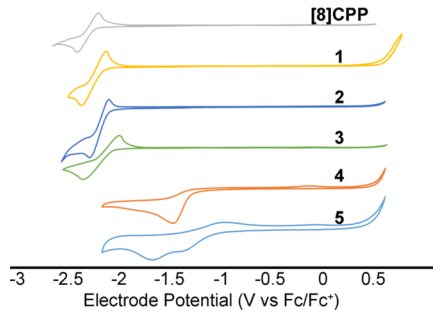

Figure 4. Cyclic Voltammetry of [8]CPP and **1–5**.

In order to better understand these effects, we turned to density function theory (DFT) computational analysis (Figure 5). As nitrogen content increases, calculations show a steady decrease in both HOMO and LUMO energies of approximately 0.07 eV from [8]CPP to **1**, **2**, and **3**. Visualization of the HOMO and LUMO orbitals showed nearly complete delocalization around the entire hoop showing a slight increase in the orbital coefficient around the nitrogen containing rings. The similar lowering of both the HOMO and LUMO orbital energies can be rationalized by the similar coefficients localized on the nitrogen for either frontier orbital. Although this nitrogen doping can fine-tune the orbitals energies, it is not sufficient to dramatically alter either the HOMO or LUMO.

Alkylation of these compounds, however, results in a dramatic shifting to less negative cathodic peak potentials in accordance with DFT predictions (Figure 5). Alkylated

DOI: 10.1021/acscentsci.5b00269
ACS Cent. Sci. 2015, 1, 335–342

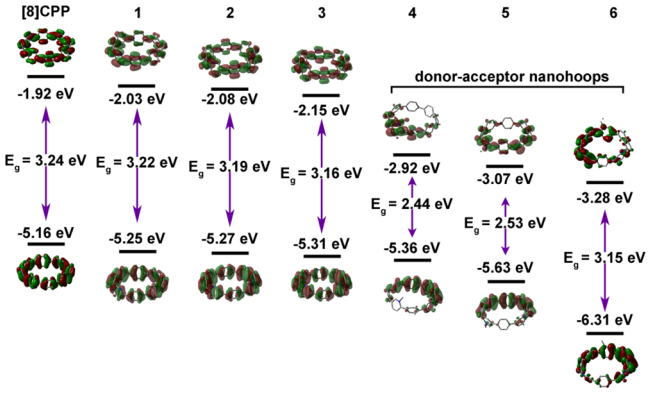

Figure 5. DFT calculated HOMO and LUMO energy levels and orbital distributions for [8]CPP and nanohoops **1**–**6**.

compounds **4** and **5** as well as computationally investigated compound *N*,*N*,*N*-trimethyl-1,15,31-triaza[8]CPP (**6**) show a dramatic lowering of the LUMO energy level by 1.00, 1.15, and 1.36 eV respectively relative to [8]CPP. This trend again follows the experimental reduction values for **4** and **5**, which show a dramatic lowering of the cathodic peak potential. Advantageously, this lowering effect was less impactful on the HOMO energy levels of nanohoop **4** and **5**, resulting in a decreased HOMO energy by only 0.200 and 0.470 eV, respectively, and a net narrowing of the HOMO–LUMO energy gap. In contrast, the theoretical triply alkylated **6** HOMO energy is lowered substantially by 1.15 eV. Visualization of the HOMO and LUMO orbitals helps explain these trends. In both the mono- and bis-alkylated structures, **4** and **5**, there is a significant dipole moment and localization of the LUMO on the *N*-methylpyridinium core. The HOMO meanwhile is localized on the bent, electron-rich phenylene backbone with orbital coefficients reaching the highest values directly opposite the *N*-methylpyridinium rings. Because of minimal contribution from the *N*-methylpyridinium core, the HOMO energies of **4** and **5** are very similar to neutral analogues **1**–**3**, as well as [8]CPP. The separation of the HOMO and LUMO orbital densities is consistent with a donor–acceptor nanohoop motif (vide infra). The calculated triply alkylated **6** on the other hand has a much lower dipole moment, and the HOMO and LUMO orbitals are localized evenly over both the phenylene and pyridinium sections. This results in a simultaneous lowering of the HOMO and LUMO orbital energies by over 1 eV therefore maintaining a similar HOMO–LUMO energy gap as the parent compound 1,15,31-triaza[8]CPP (**3**). These results suggest that the position of the *N*-methylpyridinium rings in relation to one another plays a dramatic role in modulation of the frontier molecular orbital energies (vida infra).

Optical Properties of Aza- and Donor–Acceptor Nanohoops. All [*n*]CPPs share a common absorbance maximum at 340 nm and show little if any absorbance in the visible spectrum.[5b] We sought to explore the impact of nitrogen and donor–acceptor incorporation on the optical properties of nanohoops. The UV–vis absorption and fluorescence spectra of [8]CPP and compounds **1**–**3** in dichloromethane (DCM) are depicted in Figure 6. Time-dependent density functional theory (TD-DFT) was used to gain a more in depth understanding of the photophysical trends with major transitions depicted in Figure 7. Orbital contributions to major and minor absorbances are outlined in the Supporting Information Tables 1–3. The major absorption for [8]CPP is 340 nm (ε = 1.0 × 10^5 M^{-1} cm^{-1}). This absorbance is comprised of four degenerate transitions, HOMO → LUMO +1, HOMO → LUMO+2, HOMO−1 → LUMO, and HOMO−2 → LUMO (red transitions in Figure 7a). Although the HOMO → LUMO transition is formally Laporte forbidden with conservation of HOMO and LUMO orbital symmetry, it is still observed as a slight shoulder centered at 400 nm (ε = 8.5 × 10^2 M^{-1} cm^{-1}) (purple transition in Figure 7a). The addition of nitrogen breaks the symmetry of the molecule and thus the degeneracy between the HOMO-1 and HOMO-2 as well as the LUMO-1 and LUMO-2 orbital energies. Increasing nitrogen content in **1**, **2**, and **3** leads to a slight red-shifting of major absorbance to 345 nm (ε = 2.5 × 10^5 M^{-1} cm^{-1}), 349 nm (ε = 7.30 × 10^5 M^{-1} cm^{-1}), and 353 nm (ε = 8.94 × 10^5 M^{-1} cm^{-1}) respectively. These absorbances are attributed to the same combination of the HOMO-1 → LUMO, HOMO-2 → LUMO, HOMO → LUMO+1, and HOMO → LUMO+2 transitions (red transitions in Figure 7b) as observed for [8]CPP. The slight red-shifting of these transitions relative to [8]CPP can be accounted for by the increasing electronegative nitrogen content having a slightly greater effect on the LUMO than the HOMO. The shoulder peaks for [8]CPP and aza CPPs **1**–**3** around 400 nm have a measured extinction coefficient (ε) of 2.5 × 10^3 M^{-1} cm^{-1}, 7.3 × 10^3 M^{-1} cm^{-1}, and 8.9 × 10^3 M^{-1} cm^{-1}, respectively. These lower energy transitions are assigned to the HOMO–LUMO absorbances (purple transitions in Figure 7b) which have larger oscillator strengths and extinction coefficients over an order of magnitude larger than observed for [8]CPP. The emission for [8]CPP was

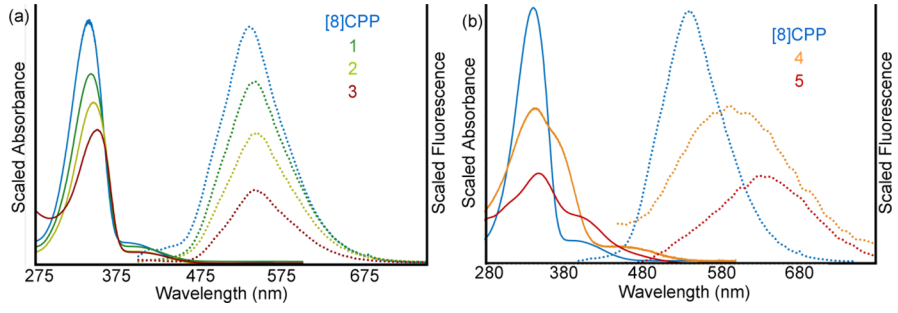

Figure 6. (a) Scaled (for clarity) UV–vis absorbance (solid lines) and fluorescence (dashed lines) of compounds [8]CPP (blue), aza[8]CPP **1** (green), 1,15-diaza[8]CPP **2** (yellow), and 1,15,31-triaza[8]CPP **3** (red) in dichloromethane. (b) Scaled (for clarity) UV–vis(solid lines) and fluorescence (dashed lines) for compounds [8]CPP (blue), *N*-methylaza[8]CPP triflate **4** (orange), and *N*,*N*-dimethyl-1,15-diaza[8]CPP ditriflate **5** (red) in dichloromethane.

DOI: 10.1021/acscentsci.5b00269
ACS Cent. Sci. 2015, 1, 335–342

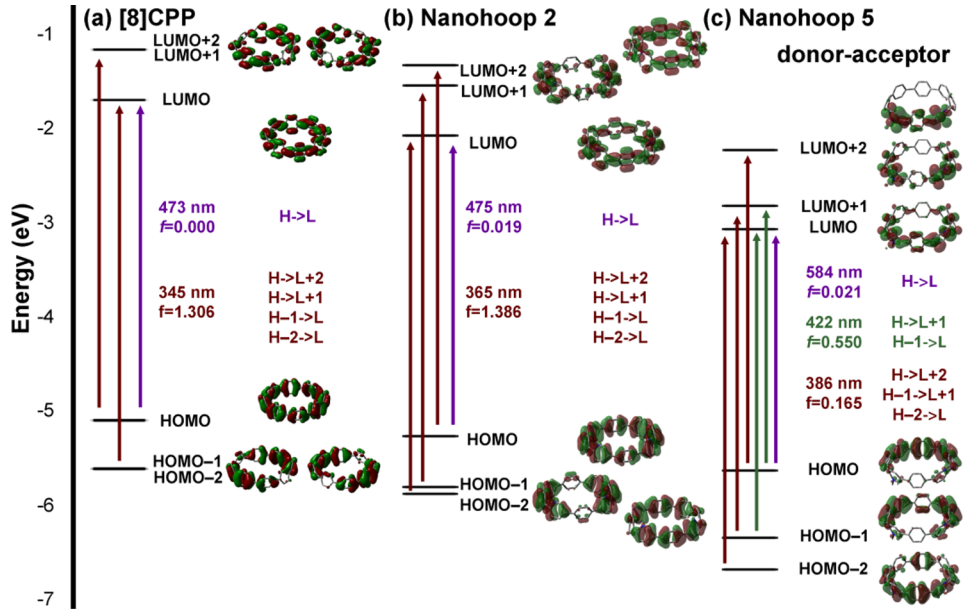

Figure 7. TD-DFT orbital transitions for (a) [8]CPP, (b) 1,15-diaza[8]CPP **2**, and (c) *N*,*N*-dimethyl-1,15-diaza[8]CPP ditriflate **5**. Pictorial orbital transitions for **1**, **3**, and **4** are found in Supplementary Figure 17. Full orbital transitions for compounds **1**−**5** are found in Supplementary Tables 1−5.

Table 1. Experimental Cathodic Peak Potentials, Maximum Absorbance, Extinction Coefficients, and Emission Maxima for [8]CPP and 1−5

compound	cathodic peak potential Fc/Fc+ (V)	max absorbance (nm)	extinction coefficient (M^{-1} cm^{-1})	emission maximum (nm)
[8]CPP	−2.44	341	1.00×10^5	533
1	−2.39	345	2.81×10^4	541
2	−2.32	349	9.21×10^4	544
3	−2.39	353	1.13×10^4	542
4	−1.49	345	2.90×10^4	598
5	−1.36	350	4.91×10^4	630

reported at 533 nm.[20] In accordance with the red-shifted absorbance, the fluorescence for compounds **1**, **2**, and **3** are slightly shifted to 541, 544, and 542 nm, respectively. Similar to the solid-state packing and cathodic peak potentials, simple nitrogen incorporation has a marginal effect on the photophysical properties of these compounds. This minimal modulation of optical and electronic properties is consistent with other reported modified nanohoops that have high symmetry.

A more prominent change is observed upon alkylation of the aza-nanohoops. Absorbance and emission spectra for alkylated compounds **4** and **5** are depicted in Figure 6b. TD-DFT transitions are summarized in Supporting Information Tables 4 and 5. The greater disparity in the relevant molecular orbital energies leads to three distinct absorbing regions. The major absorbance and highest energy transitions for **4** and **5** are at 345 nm ($\varepsilon = 2.90 \times 10^4$ M^{-1} cm^{-1}) and 350 nm ($\varepsilon = 4.91 \times 10^4$ M^{-1} cm^{-1}) respectively and correspond to the higher energy HOMO-2 → LUMO and HOMO → LUMO+2 transitions (red transitions in Figure 7c). The second absorbing region is lower in energy and appears in the visible spectrum as a shoulder peak for **4** and **5** between 400 and 425 nm. These can be assigned to the lower energy HOMO → LUMO+1 and HOMO−1 → LUMO transitions (green transitions in Figure 7c). The HOMO → LUMO transitions (purple transitions in Figure 5) are calculated to have low, yet nonzero oscillator strengths and are still orbital symmetry forbidden. This peak is observed as a weak low energy feature at 460 and 554 nm for **4** and **5** respectively. Although alkylated compounds **4** and **5** were nearly nonemissive, a red-shifted fluorescence was observed at 598 and 630 nm, respectively. This is nearly a 100 nm shift from the formally neutral species, which emit around 542 nm. This correlates well with the theoretical difference in the HOMO−LUMO energy gap between the neutral compound ([8]CPP and **1**−**3**) and the alkylated compounds (**4** and **5**). This observation supports the theory that emission likely occurs from the lowest energy excited S_1 state in accordance with Kasha's rule or a related, vibrationally relaxed excited state $S_{1'}$ as postulated by Tretiak et al.[21]

METHODS

The synthesis and characterization of all new compounds were executed by standard methods and are fully described in the Supporting Information. The effects of nitrogen incorporation on the electronic structure and properties of [8]CPP were explored in detail for the target molecules **1**−**5** using DFT calculations at the B3LYP/6-31g* level of theory using *Gaussian 09*.[15] Ground state geometry optimizations were first performed in the gas phase. Although geometries and orbital densities from these calculations have been shown to correlate well with experimental values, the addition of charged species are known to give inaccurate values for orbital energies. In the gas phase, charged species have high electrostatic interactions, which cause the calculated orbital energies to be

DOI: 10.1021/acscentsci.5b00269
ACS Cent. Sci. 2015, 1, 335−342

inaccurate. Mujica et al. recently showed that this discrepancy can be corrected by minimizing each geometry in the gas phase while omitting the counterion for charged species.[16] A solvated (acetonitrile) single point energy calculation is then performed using the conductor-like polarization continuum model (CPCM). This method gives stronger correlation between computed frontier orbitals and experimental reduction and oxidation values for both charged and neutral aromatic species. In accordance with this report, all compounds in this work were treated with the outlined workflow described above. TD-DFT was used to predict and assign optical absorbances again using CPCM with acetonitrile as the solvent. The computed values are red-shifted in relation to the experimental spectra. This trend is commonly observed; however, the peak shape and relative intensity matched the experimental results allowing assignment of optical transitions.

SIGNIFICANCE AND OUTLOOK

At the outset of this project, we aimed to use nitrogen incorporation to theoretically and experimentally explore the impact on the HOMO and LUMO energy levels of nanohoops. Gratifyingly, we were able to elucidate a strategy which, in the case of highly polarized compounds **4** and **5**, can lower the LUMO energy independent of the HOMO energy resulting in a net lowering of the HOMO-LUMO energy gap. The LUMO orbital energy levels achieved through alkylation of the aza[8]CPP are on the cusp of the desirable range of −3.0 eV to −4.0 eV for use as organic electronic materials.[22] Also we find that by incorporating multiple *N*-methylpyridinium units in a highly symmetric structure (**6**) we are able to drop both the LUMO and HOMO energies equally, a feature that is important when designing organic devices with high open circuit voltages (V_{oc}). With these results and a basic understanding in hand, we attempted to further probe the concept of the donor−acceptor nanohoop in order to guide future design.

With the difficulties associated with the synthesis of triply alkylated structure **6**, we sought to explore the possibility of attaining similar HOMO−LUMO energy levels by changing the relative positioning in the doubly alkylated diaza[8]CPP scaffold. This effect was computationally studied by changing the relative pyridinium position in the *N*,*N*-dimethyl-*x*,*y*-diaza[8]CPP scaffold where *x* and *y* represent the relative position of each nitrogen in the hoop (Figure 8). The three regioisomers shown, in addition to compound **5**, highlight the importance of the relative positioning of the acceptor groups. The (1,8) isomer (Figure 8, left) has the lowest lying LUMO with orbital localization primarily on the electron-poor pyridinium rings. The HOMO remains localized on the bent, electron-rich phenylene backbone maintaining an energy closer to neutral compound **5**. This gives a HOMO−LUMO energy gap of 1.7 eV, a value that coincides with a significant increase in the calculated absorption in the visible spectrum (Supplementary Figure 18). When the pyridinium rings are opposite one another in the (1,27) position (Figure 8, right), a significant increase in orbital coefficients is observed for the HOMO and LUMO on both the pyridinium and phenylene sections resulting in a lowering of both energies, while maintaining a HOMO−LUMO energy gap around 3.0 eV. These results emphasize the need to construct nanohoops with high dipole moments rather than high symmetry, as has been primarily investigated, in order to attain low HOMO−LUMO energy gap materials.[13b,23] This aspect offers yet another

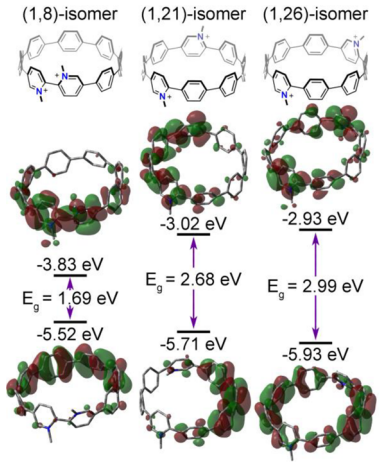

Figure 8. Theoretical HOMO and LUMO energies for (left) *N*,*N*-dimethyl-1,8-diaza[8]CPP, (center) *N*,*N*-dimethyl-1,21-diaza[8]CPP, and (right) *N*,*N*-dimethyl-1,26-diaza[8]CPP.

control element when designing future donor−acceptor nanohoops.

The use of alternating donor and acceptor moieties in organic materials is ubiquitous in both polymeric and small molecule organic electronics and is often used to construct chromophores and narrow HOMO−LUMO energy gaps.[24] In the current study, the *N*-methylpyridinium ring acts as the acceptor, and the strained paraphenylene backbone serves as the donor. To assess the generality of this finding, we computationally explored a common donor benzodithiophene (BTD) and acceptor benzothiadiazole (BT) in the context of [6]cycloparaphenylene ([6]CPP) and linear [6]oligophenylene ([6]OPP) (Figure 9). As shown, [6]CPP has a 1.01 eV

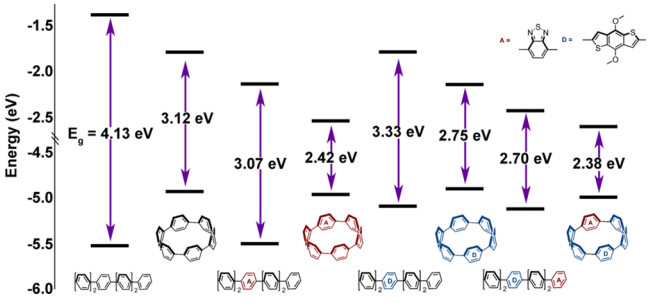

Figure 9. Effect of acceptor (red), donor (blue), and donor−acceptor moieties on the HOMO and LUMO energies of [6]CPP and linear [6]OPP frameworks.

narrower HOMO−LUMO energy gap compared to [6]OPP. As expected, the LUMO energy drops for both [6]OPP and [6]CPP when the acceptor BT is incorporated. Interestingly, the addition of the donor BTD leads to a raising of the HOMO energy for the linear [6]OPP, but has little to no effect on the cyclic [6]CPP. Finally, incorporation of both the donor BTD and the acceptor BT leads to a raising of the HOMO energy and lowering in the LUMO energy for the linear [6]OPP, but only a lowering of the LUMO energy in the case of the cyclic [6]CPP. The HOMO−LUMO energy gap for the donor−acceptor [6]OPP drops to 2.70 eV, while the HOMO−LUMO energy gap for the donor−acceptor cyclic [6]CPP remains nearly identical to the BT substituted [6]CPP. This result suggests that the bent CPP backbone itself is a good donor and

DOI: 10.1021/acscentsci.5b00269
ACS Cent. Sci. 2015, 1, 335−342

that addition of complex donor heterocycles is unnecessary therefore simplifying synthetic efforts toward donor−acceptor nanohoops. Advantageously, the bent phenylene backbone acts as a good donor on its own where donor strength can be tuned by changing the size of the hoop. These findings highlight the importance of exploring acceptor-containing nanohoops in future materials.

CONCLUSION

In conclusion, the modular syntheses of aza[8]CPPs were developed in order to probe the impact of nitrogen doping on nanohoop optical, electronic, and solid state properties. Increasing nitrogen content led to a slight red shifting in both the absorbance and fluorescence and dropped the cathodic peak potential for reduction on average by 0.07 V. Similar to its modulation of the optical and electronic properties, nitrogen content had little influence on the solid state structure of the nanohoops. Further alkylation of these aza-nanhoops, however, afforded donor−acceptor nanohoops resulting in increased absorbance in the visible spectrum and over a 0.5 V decrease in cathodic peak potential. The high dipole moment (through-bond and through-space) of the alkylated aza-nanohoops afforded topologically unique solid-state nanohoop packings. The synthesis and characterization of these aza-nanohoops have led to a deeper understanding of the impact of structural modification on the optical and electronic properties of these nanohoops. We find that incorporation of electron-poor acceptors has a more dramatic effect on the electronic structure of nanohoops than incorporation of electron-rich moieties. This feature implies that the bent phenylene architecture intrinsically acts as a good donor, and donor strength can be tuned by nanohoop size. In addition, relative positioning of multiple acceptor groups leads to nanohoops with dramatically different properties. With the ability to modularly construct novel nanohoops and with emerging strategies to introduce functional groups in a mild manner, we have begun to target and examine the donor−acceptor structures with the most promising electronic features.[5,25] We anticipate that the donor−acceptor nanohoop architecture will be an important additional tool in the organic materials chemistry tool box.

ASSOCIATED CONTENT

Supporting Information

The Supporting Information is available free of charge on the ACS Publications website at DOI: 10.1021/acscentsci.5b00269.

Experimental details and procedures; NMR spectra; crystallographic information; photophysical data; TD-DFT transitions; computational coordinates (PDF)

AUTHOR INFORMATION

Corresponding Author

*E-mail: rjasti@uoregon.edu.

Notes

The authors declare no competing financial interest.

ACKNOWLEDGMENTS

Financial support was provided by the National Science Foundation (CHE-1255219), the Sloan Foundation, the Camille and Henry Dreyfus Foundation, and generous startup funds from the University of Oregon. E.S.H thanks the AAUW for their graduate fellowship support. C.D.W. and M.C.L. acknowledge the Division of Chemical Sciences, Geosciences and Biosciences, Office of Basic Energy Sciences of the U.S. Department of Energy through Grant DE-SC0012363 for supporting the electrochemistry work. The authors would like to gratefully acknowledge Eric P. Boon (Stevens Institute of Technology) for experimental assistance, Dalvin D. Méndez-Hernández (Yale) for computational assistance, and Dr. Jeffrey W. Bacon (Boston University) for assistance with X-ray crystallography of compound **8a**.

REFERENCES

(1) Lewis, N. S.; Nocera, D. G. Powering the planet: Chemical challenges in solar energy utilization. *Proc. Natl. Acad. Sci. U. S. A.* **2006**, *103* (43), 15729−15735.

(2) Anthony, J. E. Functionalized Acenes and Heteroacenes for Organic Electronics. *Chem. Rev.* **2006**, *106* (12), 5028−5048.

(3) (a) McQuade, D. T.; Pullen, A. E.; Swager, T. M. Conjugated Polymer-Based Chemical Sensors. *Chem. Rev.* **2000**, *100* (7), 2537−2574. (b) Izuhara, D.; Swager, T. M. Bispyridinium-phenylene-based copolymers: low band gap n-type alternating copolymers. *J. Mater. Chem.* **2011**, *21* (11), 3579−3584. (c) Izuhara, D.; Swager, T. M. Poly(Pyridinium Phenylene)s: Water-Soluble N-Type Polymers. *J. Am. Chem. Soc.* **2009**, *131* (49), 17724−17725.

(4) Brédas, J. L.; Calbert, J. P.; da Silva Filho, D. A.; Cornil, J. Organic semiconductors: A theoretical characterization of the basic parameters governing charge transport. *Proc. Natl. Acad. Sci. U. S. A.* **2002**, *99* (9), 5804−5809.

(5) (a) Golder, M. R.; Jasti, R. Syntheses of the Smallest Carbon Nanohoops and the Emergence of Unique Physical Phenomena. *Acc. Chem. Res.* **2015**, *48* (3), 557−566. (b) Darzi, E. R.; Jasti, R. The dynamic, size-dependent properties of [5]-[12]cycloparaphenylenes. *Chem. Soc. Rev.* **2015**, *44*, 6401.

(6) Brédas, J. L.; Heeger, A. J. Influence of donor and acceptor substituents on the electronic characteristics of poly(paraphenylene vinylene) and poly(paraphenylene). *Chem. Phys. Lett.* **1994**, *217* (5−6), 507−512.

(7) Iwamoto, T.; Watanabe, Y.; Sakamoto, Y.; Suzuki, T.; Yamago, S. Selective and Random Syntheses of [*n*]Cycloparaphenylenes (*n* = 8−13) and Size Dependence of Their Electronic Properties. *J. Am. Chem. Soc.* **2011**, *133* (21), 8354−8361.

(8) Segawa, Y.; Omachi, H.; Itami, K. Theoretical Studies on the Structures and Strain Energies of Cycloparaphenylenes. *Org. Lett.* **2010**, *12* (10), 2262−2265.

(9) Alvarez, M. P.; Burrezo, P. M.; Kertesz, M.; Iwamoto, T.; Yamago, S.; Xia, J.; Jasti, R.; Navarrete, J. T. L.; Taravillo, M.; Baonza, V. G.; Casado, J. Properties of Sizeable [*n*]Cycloparaphenylenes as Molecular Models of Single-Wall Carbon Nanotubes Elucidated by Raman Spectroscopy: Structural and Electron-Transfer Responses under Mechanical Stress. *Angew. Chem., Int. Ed.* **2014**, *53* (27), 7033−7037.

(10) Unsubstituted linear [*n*]oligoparaphenylenes become completely insoluble when *n* > 6.

(11) (a) Takase, M.; Narita, T.; Fujita, W.; Asano, M. S.; Nishinaga, T.; Benten, H.; Yoza, K.; Müllen, K. Pyrrole-Fused Azacoronene Family: The Influence of Replacement with Dialkoxybenzenes on the Optical and Electronic Properties in Neutral and Oxidized States. *J. Am. Chem. Soc.* **2013**, *135* (21), 8031−8040. (b) Berger, R.; Giannakopoulos, A.; Ravat, P.; Wagner, M.; Beljonne, D.; Feng, X.; Müllen, K. Synthesis of Nitrogen-Doped ZigZag-Edge Peripheries: Dibenzo-9a-azaphenalene as Repeating Unit. *Angew. Chem., Int. Ed.* **2014**, *53* (39), 10520−10524. (c) Ito, S.; Tokimaru, Y.; Nozaki, K. Benzene-Fused Azacorannulene Bearing an Internal Nitrogen Atom. *Angew. Chem., Int. Ed.* **2015**, *54* (25), 7256−7260.

(12) (a) Keshavarz-K, M.; Gonzalez, R.; Hicks, R. G.; Srdanov, G.; Srdanov, V. I.; Collins, T. G.; Hummelen, J. C.; Bellavia-Lund, C.; Pavlovich, J.; Wudl, F.; Holczer, K. Synthesis of hydroazafullerene C59HN, the parent hydroheterofullerene. *Nature* **1996**, *383* (6596), 147−150. (b) Chen, P.; Chew, L. M.; Kostka, A.; Muhler, M.; Xia, W.

DOI: 10.1021/acscentsci.5b00269
ACS Cent. Sci. 2015, 1, 335−342

The structural and electronic promoting effect of nitrogen-doped carbon nanotubes on supported Pd nanoparticles for selective olefin hydrogenation. *Catal. Sci. Technol.* **2013**, *3* (8), 1964−1971. (c) Stephan, O.; Ajayan, P. M.; Colliex, C.; Redlich, P.; Lambert, J. M.; Bernier, P.; Lefin, P. Doping Graphitic and Carbon Nanotube Structures with Boron and Nitrogen. *Science* **1994**, *266* (5191), 1683−1685.

(13) (a) Matsui, K.; Segawa, Y.; Itami, K. Synthesis and Properties of Cycloparaphenylene-2,5-pyridylidene: A Nitrogen-Containing Carbon Nanoring. *Org. Lett.* **2012**, *14* (7), 1888−1891. (b) Ito, H.; Mitamura, Y.; Segawa, Y.; Itami, K. Thiophene-Based, Radial π-Conjugation: Synthesis, Structure, and Photophysical Properties of Cyclo-1,4-phenylene-2′,5′-thienylenes. *Angew. Chem., Int. Ed.* **2015**, *54* (1), 159−163. (c) Huang, C.; Huang, Y.; Akhmedov, N. G.; Popp, B. V.; Petersen, J. L.; Wang, K. K. Functionalized Carbon Nanohoops: Synthesis and Structure of a [9]Cycloparaphenylene Bearing Three 5,8-Dimethoxynaphth-1,4-diyl Units. *Org. Lett.* **2014**, *16* (10), 2672−2675. (d) Tran-Van, A.-F.; Huxol, E.; Basler, J. M.; Neuburger, M.; Adjizian, J.-J.; Ewels, C. P.; Wegner, H. A. Synthesis of Substituted [8]Cycloparaphenylenes by [2 + 2 + 2] Cycloaddition. *Org. Lett.* **2014**, *16* (6), 1594−1597. (e) Tran-Van, A.-F.; Wegner, H. A. Nano-rings with a handle − Synthesis of substituted cycloparaphenylenes. *Beilstein J. Nanotechnol.* **2014**, *5*, 1320−1333. (f) Bachrach, S. M.; Stück, D. DFT Study of Cycloparaphenylenes and Heteroatom-Substituted Nanohoops. *J. Org. Chem.* **2010**, *75* (19), 6595−6604.

(14) During the preparation of this manuscript, two related concepts were reported. The first was reported by Nuckolls et al. Ball, M.; Fowler, B.; Li, P.; Joyce, L. A.; Li, F.; Liu, T.; Paley, D.; Zhong, Y.; Li, H.; Xiao, S.; Ng, F.; Steigerwald, M. L.; Nuckolls, C. Chiral Conjugated Corrals. *J. Am. Chem. Soc.* **2015**, *137* (31), 9982−9987. The second was reported by Itami et al. Kuwabara, T.; Orii, J.; Segawa, Y.; Itami, K. Curved Oligophenylenes as Donors in Shape-Persistent Donor−Acceptor Macrocycles with Solvatofluorochromic Properties. *Angew. Chem.* **2015**, *127* (33), 9782−9785.

(15) Frisch, M. J. T, G. W.; Schlegel, H. B.; Scuseria, G. E.; Robb, M. A.; Cheeseman, J. R.; Scalmani, G.; Barone, V.; Mennucci, B.; Petersson, G. A.; Nakatsuji, H.; Caricato, M.; Li, X.; Hratchian, H. P.; Izmaylov, A. F.; Bloino, J.; Zheng, G.; Sonnenberg, J. L.; Hada, M.; Ehara, M.; Toyota, K.; Fukuda, R.; Hasegawa, J.; Ishida, M.; Nakajima, T.; Honda, Y.; Kitao, O.; Nakai, H.; Vreven, T.; Montgomery, J. A., Jr.; Peralta, J. E.; Ogliaro, F.; Bearpark, M.; Heyd, J. J.; Brothers, E.; Kudin, K. N.; Staroverov, V. N.; Kobayashi, R.; Normand, J.; Raghavachari, K.; Rendell, A.; Burant, J. C.; Iyengar, S. S.; Tomasi, J.; Cossi, M.; Rega, N.; Millam, N. J.; Klene, M.; Knox, J. E.; Cross, J. B.; Bakken, V.; Adamo, C.; Jaramillo, J.; Gomperts, R.; Stratmann, R. E.; Yazyev, O.; Austin, A. J.; Cammi, R.; Pomelli, C.; Ochterski, J. W.; Martin, R. L.; Morokuma, K.; Zakrzewski, V. G.; Voth, G. A.; Salvador, P.; Dannenberg, J. J.; Dapprich, S.; Daniels, A. D.; Farkas, Ö.; Foresman, J. B.; Ortiz, J. V.; Cioslowski, J.; Fox, D. J. *Gaussian 09*, Revision D.01; Gaussian: Wallingford, CT, 2009.

(16) Méndez-Hernández, D. D.; Gillmore, J. G.; Montano, L. A.; Gust, D.; Moore, T. A.; Moore, A. L.; Mujica, V. Building and testing correlations for the estimation of one-electron reduction potentials of a diverse set of organic molecules. *J. Phys. Org. Chem.* **2015**, *28* (5), 320−328.

(17) (a) Evans, P. J.; Darzi, E. R.; Jasti, R. Efficient room-temperature synthesis of a highly strained carbon nanohoop fragment of buckminsterfullerene. *Nat. Chem.* **2014**, *6*, 404. (b) Xia, J.; Bacon, J. W.; Jasti, R. Gram-scale synthesis and crystal structures of [8]- and [10]CPP, and the solid-state structure of C60@[10]CPP. *Chem. Sci.* **2012**, *3* (10), 3018−3021. (c) Darzi, E. R.; Sisto, T. J.; Jasti, R. Selective Syntheses of [7]−[12]Cycloparaphenylenes Using Orthogonal Suzuki−Miyaura Cross-Coupling Reactions. *J. Org. Chem.* **2012**, *77* (15), 6624−6628. (d) Sisto, T. J.; Golder, M. R.; Hirst, E. S.; Jasti, R. Selective Synthesis of Strained [7]Cycloparaphenylene: An Orange-Emitting Fluorophore. *J. Am. Chem. Soc.* **2011**, *133* (40), 15800−15802. (e) Jasti, R.; Bhattacharjee, J.; Neaton, J. B.; Bertozzi, C. R. Synthesis, Characterization, and Theory of [9]-, [12]-, and [18]-Cycloparaphenylene: Carbon Nanohoop Structures. *J. Am. Chem. Soc.* **2008**, *130* (52), 17646−17647.

(18) (a) Cai, D.; Hughes, D. L.; Verhoeven, T. R. A study of the lithiation of 2,6-dibromopyridine with butyllithium, and its application to synthesis of L-739,010. *Tetrahedron Lett.* **1996**, *37* (15), 2537−2540. (b) Wang, X.; Rabbat, P.; O'Shea, P.; Tillyer, R.; Grabowski, E. J. J.; Reider, P. J. Selective monolithiation of 2,5-dibromopyridine with butyllithium. *Tetrahedron Lett.* **2000**, *41* (22), 4335−4338.

(19) Xia, J.; Jasti, R. Synthesis, Characterization, and Crystal Structure of [6]Cycloparaphenylene. *Angew. Chem., Int. Ed.* **2012**, *51* (10), 2474−2476.

(20) Yamago, S.; Watanabe, Y.; Iwamoto, T. Synthesis of [8]Cycloparaphenylene from a Square-Shaped Tetranuclear Platinum Complex. *Angew. Chem., Int. Ed.* **2010**, *49* (4), 757−759.

(21) (a) Adamska, L.; Nayyar, I.; Chen, H.; Swan, A. K.; Oldani, N.; Fernandez-Alberti, S.; Golder, M. R.; Jasti, R.; Doorn, S. K.; Tretiak, S. Self-Trapping of Excitons, Violation of Condon Approximation, and Efficient Fluorescence in Conjugated Cycloparaphenylenes. *Nano Lett.* **2014**, *14* (11), 6539−6546. (b) Kasha, M. Characterization of electronic transitions in complex molecules. *Discuss. Faraday Soc.* **1950**, *9* (0), 14−19.

(22) Duan, C.; Huang, F.; Cao, Y. Recent development of push-pull conjugated polymers for bulk-heterojunction photovoltaics: rational design and fine tailoring of molecular structures. *J. Mater. Chem.* **2012**, *22* (21), 10416−10434.

(23) Iwamoto, T.; Kayahara, E.; Yasuda, N.; Suzuki, T.; Yamago, S. Synthesis, Characterization, and Properties of [4]Cyclo-2,7-pyrenylene: Effects of Cyclic Structure on the Electronic Properties of Pyrene Oligomers. *Angew. Chem., Int. Ed.* **2014**, *53* (25), 6430−6434.

(24) Lin, Y.; Li, Y.; Zhan, X. Small molecule semiconductors for high-efficiency organic photovoltaics. *Chem. Soc. Rev.* **2012**, *41* (11), 4245−4272.

(25) (a) Kubota, N.; Segawa, Y.; Itami, K. η6-Cycloparaphenylene Transition Metal Complexes: Synthesis, Structure, Photophysical Properties, and Application to the Selective Monofunctionalization of Cycloparaphenylenes. *J. Am. Chem. Soc.* **2015**, *137* (3), 1356−1361. (b) Patel, V. K.; Kayahara, E.; Yamago, S. Practical Synthesis of [n]Cycloparaphenylenes (n = 5, 7−12) by H_2SnCl_4-Mediated Aromatization of 1,4-Dihydroxycyclo-2,5-diene Precursors. *Chem. - Eur. J.* **2015**, *21* (15), 5742−5749.

DOI: 10.1021/acscentsci.5b00269
ACS Cent. Sci. 2015, 1, 335−342